Journal of Solid State Chemistry **142,** 400–408 (1999)
Article ID jssc.1998.8055, available online at http://www.idealibrary.com on IDEAL®

Crystal Structure and Magnetic Properties of the Lanthanoid Platinum Germanides *Ln*PtGe (*Ln* = Ce, Pr, Nd, Sm)

Yurij M. Prots', Rainer Pöttgen, Dirk Niepmann, Michael W. Wolff, and Wolfgang Jeitschko[1]

Anorganisch-Chemisches Institut, Universität Münster, Wilhelm-Klemm-Straße 8, D-48149 Münster, Germany

Received August 27, 1998; accepted October 5, 1998

DEDICATED TO PROFESSOR H. D. LUTZ ON THE OCCASION OF HIS 65TH BIRTHDAY

The crystal structures of the title compounds were reinvestigated. The previously reported KHg_2 ($CeCu_2$) type structure with statistical distribution of the platinum and germanium atoms corresponds only to the subcell of the ordered orthorhombic YPdSi type structure (*Pmmn*, $Z = 8$) of these compounds, which was refined from single-crystal X-ray diffractometer data of CePtGe: $a = 445.0(1)$ pm, $b = 1464.8(3)$ pm, $c = 761.8(2)$ pm; PrPtGe: $a = 444.01(3)$ pm, $b = 1456.57(9)$ pm, $c = 761.71(5)$ pm; and the low-temperature (α) modification of SmPtGe: $a = 440.0(1)$ pm, $b = 1428.1(2)$ pm, $c = 756.6(1)$ pm. Nevertheless, some evidence for disorder was obtained from the refinement of the occupancy parameters of these compounds. The results suggest the substitution of germanium by platinum atoms and/or vice versa in the order of a few at%. The high-temperature (β) modification of SmPtGe with TiNiSi type structure was confirmed by a refinement from single crystal diffractometer data. The magnetic properties of these compounds were investigated with a SQUID magnetometer. CePtGe, PrPtGe, and NdPtGe follow the Curie–Weiss law with magnetic moments close to those of the trivalent rare earth elements. The magnetic properties of α- and β-SmPtGe are dominated by the Van Vleck paramagnetism of the samarium atoms. Antiferromagnetic ordering was detected for CePtGe, NdPtGe, and both modifications of SmPtGe with Néel temperatures between 4 and 6 K, while PrPtGe remains paramagnetic down to 2 K. The crystal structures of these compounds are briefly discussed together with those of the LaPtSi and LaIrSi type structures, which occur for LaPtGe and EuPtGe, respectively.

Key Words: **rare earth compounds, germanides, crystal structure, superstructure, order–disorder, magnetic properties.**

INTRODUCTION

The series of equiatomic rare earth platinum germanides has been investigated for some time. LaPtGe was found to be isotypic with LaPtSi (1). In this structure the platinum and silicon atoms occupy the silicon positions of the well-known α-$ThSi_2$ type structure in an ordered manner (2). The compounds *R*PtGe (*R* = Sc, Y, Sm, Gd–Tm) are isotypic with TiNiSi, a structure which may be considered as a distorted version of the hexagonal Ni_2In type structure (3, 4). Alternately it may also be regarded as an ordered version of the binary KHg_2 ($CeCu_2$) structure type (1, 5). The europium compound EuPtGe (6, 7) crystallizes with LaIrSi type structure, which has been described as an ordered $SrSi_2$ derivative structure (8). In contrast, a disordered KHg_2 ($CeCu_2$) type structure has been assumed for the compounds *Ln*PtGe (*Ln* = Ce, Nd, Pr, Sm) (1, 9–11). We have recently reported on several superstructures with KHg_2 type subcell (12–16). In the course of our studies of equiatomic rare earth palladium silicides *Ln*PdSi (14, 16, 17) we decided to search for the suspected superstructure in the germanides *Ln*PtGe reported to be isotypic with KHg_2 ($CeCu_2$). We find that these compounds crystallize with a YPdSi type superstructure (14) with KHg_2 type subcell. In addition, we confirm the TiNiSi type structure for (β-) SmPtGe, which is stable at high temperatures, and we report on the magnetic properties of these compounds. A preliminary account on the crystal structures of these germanides has been given at a conference (18).

SAMPLE PREPARATION AND LATTICE CONSTANTS

Starting materials for the preparation of CePtGe, PrPtGe, NdPtGe, and the two modifications of SmPtGe were ingots of the rare earth elements (Johnson Matthey; Kelpin), platinum powder (Degussa, 200 mesh), and germanium lumps (Wacker), all with stated purities greater than 99.9%. In a first step, small pieces of the lanthanoid ingots were melted to buttons under argon in an arc-melting furnace in order to minimize a shattering of these elements during the violent reactions. The argon was purified over titanium sponge (900 K) and molecular sieves. The resulting

[1]To whom correspondence should be addressed. Fax: + 49-251-83-33136.

0022-4596/99 $30.00

TABLE 1
Lattice Constants of the Orthorhombic Germanides *Ln*PtGe (*Ln* = Ce–Sm)[a]

Compound	Structure type	Space gr.	*a* (pm)	*b* (pm)	*c* (pm)	*V* (nm^3)	Reference
CePtGe	YPdSi	*Pmmn*	445.0(1)	1464.8(3)	761.8(2)	0.4966(1)	This work
CePtGe	KHg_2 (subcell)	*Imma*	445.0(1)	734.7(3)	761.5(3)	0.2490(2)	(1)
CePtGe	KHg_2 (subcell)	*Imma*	445.15(8)	734.4(2)	761.6(4)	0.2490(1)	(10)
CePtGe	KHg_2 (subcell)	*Imma*	444.5(2)	732.9(3)	760.9(3)	0.2479(3)	(11)
PrPtGe	YPdSi	*Pmmn*	444.01(3)	1456.57(9)	761.71(5)	0.49262(5)	This work
PrPtGe	KHg_2 (subcell)	*Imma*	443.8(1)	729.2(2)	761.6(2)	0.2465(1)	(1)
NdPtGe	YPdSi	*Pmmn*	442.6(2)	1447.0(5)	759.9(2)	0.4867(2)	This work
NdPtGe	KHg_2 (subcell)	*Imma*	442.8(1)	724.5(2)	759.9(2)	0.2438(1)	(1)
α-SmPtGe	KHg_2 (subcell)	*Imma*	439.7(1)	714.3(1)	757.8(2)	0.2380(1)	(9)
α-SmPtGe	YPdSi	*Pmmn*	440.0(1)	1428.1(2)	756.6(1)	0.4754(1)	This work
β-SmPtGe	TiNiSi	*Pnma*	714.4(2)	439.6(1)	757.5(2)	0.2379(1)	(1)
β-SmPtGe	TiNiSi	*Pnma*	713.5(1)	438.8(1)	760.3(1)	0.2381(1)	This work

[a] Standard deviations in the positions of the least significant digits are given in parentheses throughout the paper for all crystallographic data. The settings of the three different structures have the following relations: *abc* (KHg_2) ~ *bāc* (TiNiSi) ~ *a*2*bc* (YPdSi).

lanthanoid buttons were then melted together with the germanium lumps and with the pressed pellets of platinum powder in the ideal atomic ratio 1 : 1 : 1. The buttons were turned over and remelted at least two times in order to achieve homogeneity. The total weight losses during the arc-melting procedures were smaller than 0.5% in all cases. Subsequently, parts of the melted ingots were sealed in evacuated silica ampoules and annealed at 1070 K for up to four weeks. All of these annealed samples were microcrystalline.

Well-crystallized samples of CePtGe and PrPtGe were obtained by annealing parts of the arc-melted buttons in evacuated, sealed, and water-cooled silica ampoules in a high-frequency furnace slightly below the (undetermined) melting points for about two hours. These samples were subsequently sealed in evacuated silica tubes and annealed for another three weeks at 1070 K. Crystals of β-SmPtGe were taken from the arc-melted sample, and those of α-SmPtGe were obtained after annealing at 1070 K without heat treatment in the high-frequency furnace.

The powder samples of the investigated germanides are of light gray color. They are stable in air for long periods of time. The irregularly shaped single crystals had silvery metallic luster.

Guinier powder patterns of the samples were recorded after each reaction step with Cu$K\alpha_1$ radiation using α-quartz ($a = 491.30$ pm, $c = 540.46$ pm) as an internal standard. The orthorhombic lattice constants (Table 1) were obtained from least-squares fits of the Guinier data. To assure correct indexing, the observed patterns were compared with the calculated ones (19), taking the atomic positions resulting from the structure refinements.

TABLE 2
Magnetic Data for the Germanides *Ln*PtGe (*Ln* = Ce, Pr, Nd, Sm)[a]

Compound	Magnetic behavior	μ_{exp} (μ_B/Ln^{3+})	μ_{eff} (μ_B/Ln^{3+})	Θ (K)	χ_0 m^3/mol	T_N (K)
CePtGe	Antiferro/Curie–Weiss	2.60(5)	2.54	− 89(4)	$-0.8(5)\cdot10^{-9}$	4(1)
PrPtGe	Curie–Weiss	3.66(5)	3.58	− 9(4)	$-1.1(3)\cdot10^{-9}$	—
NdPtGe	Antiferro/Curie–Weiss	3.67(5)	3.62	− 12(4)	$-0.08(3)\cdot10^{-9}$	6(1)
α-SmPtGe	Antiferro/Van Vleck para	1.88(2)	1.91	—	$13.8(3)\cdot10^{-9}$	4.5(5)
β-SmPtGe	Antiferro/Van Vleck para	1.95(2)	1.91	—	$14.9(3)\cdot10^{-9}$	4.0(5)

[a] The experimentally determined magnetic moments μ_{exp} were calculated from the relation $\mu_{eff} = 2.83\cdot C^{1/2}/(4\pi\cdot10^{-6})\,\mu_B$, where the values of C were obtained by fits of the data to the modified Curie–Weiss law $\chi = \chi_0 + C/(T - \Theta)$. They are compared with the theoretical moments μ_{eff}, calculated from the relation $\mu_{eff} = g[J(J+1)]^{1/2}\,\mu_B$. The paramagnetic Curie temperatures (Weiss constants) Θ and the Néel temperatures T_N are also listed. The experimental and the theoretical magnetic moments μ_{exp} and μ_{eff} for the two modifications of the samarium compound are compared for 400 K. The theoretical moment was calculated with the screening constant $\sigma = 34$ with the formula by Van Vleck (20). Estimated error limits in the place values of the last listed digits are given in parentheses for all magnetic data of this paper.

MAGNETIC PROPERTIES

The magnetic susceptibilities of coarse powders of all compounds were determined with a superconducting quantum interference device (SQUID, Quantum Design, Inc.) between 2 and 400 K with magnetic flux densities up to 5.5 T. Generally between 10 and 30 mg of each compound were filled into a silica tube (outer diameter 2 mm) and held in place by a cotton plug. The temperature was lowered in zero magnetic field and raised in the desired magnetic field. To check for ferromagnetic impurities the field dependence of each sample was determined at 2 K, at 50 K, and at room temperature. Only very minor amounts of such impurities were detected: in each case the magnetic susceptibilities recorded at 3 and 5.5 T were practically identical. The magnetic properties of all compounds are summarized in Table 2.

The three germanides CePtGe, PrPtGe, and NdPtGe show Curie–Weiss behavior (Fig. 1). The magnetic moments μ_{exp} determined from the slopes of the $1/\chi$ vs T plots agree well with the theoretical values μ_{eff}, calculated for the free ions Ln^{3+} (Table 2), indicating that the platinum germanium polyanions do not carry significant magnetic moments. At low temperatures antiferromagnetic order was indicated by the minima of the reciprocal susceptibilities for CePtGe and NdPtGe with Néel temperatures of 4(±1) and 6(±1) K, respectively. This was confirmed by magnetization measurements recorded at 2 K, which showed a nearly linear increase of the magnetic moments with magnetic flux densities up to 5.5 T for both compounds. The temperature independent parts χ_0 of the magnetic susceptibilities, obtained from the least-squares fits of the data to the modified Curie–Weiss law $\chi = \chi_0 + C/(T - \Theta)$ are negative. These values result from the core diamagnetism and probably are affected by the Pauli paramagnetism, since we suspect these compounds to be metallic conductors. The magnetic properties of CePtGe have already been investigated by Rogl *et al.* (10), who reported a magnetic moment of 2.54 μ_B, a Weiss constant of -82 K, and a Néel temperature of 3.4 K. Our results (Table 2) are in excellent agreement with these values.

The magnetic susceptibilities of the two modifications of SmPtGe did not follow the Curie–Weiss law, as could be expected for a compound containing the Van Vleck ion Sm^{3+}. The experimental moments of $\mu_{exp} = 1.88$ (± 0.02) μ_B/mol and $\mu_{exp} = 1.95$ (± 0.02) μ_B/mol obtained for the α- and β-modifications, respectively, from the relation $\mu_{exp} = 2.83\,(\chi \cdot T)^{1/2}/(4\pi \cdot 10^{-6})\,\mu_B$ for $T = 400$ K compare well with the value of $\mu_{eff} = 1.91\,\mu_B$, calculated with the Van Vleck formula (20) for a screening constant of $\sigma = 34$. Similarly, the minima of the magnetic susceptibilities of $\chi_0 = 13.8(\pm 0.3)\cdot 10^{-9}$ and $\chi_0 = 14.9(\pm 0.3)\cdot 10^{-9}$ m^3/mol for the α- and β-modifications of SmPtGe compare well with the average value of 13.4×10^{-9} m^3/mol Sm^{3+} found for the two modifications of Sm_2O_3 and the oxalate $Sm_2(C_2O_4)_3 \cdot 10\,H_2O$ (21). Antiferromagnetic order with Néel temperatures of 4.5 (± 0.5) and 4.0 (± 0.5) K for α-SmPtGe and β-SmPtGe, respectively, is indicated by the minima of the reciprocal susceptibility curves (Fig. 2). This was confirmed by magnetization measurements.

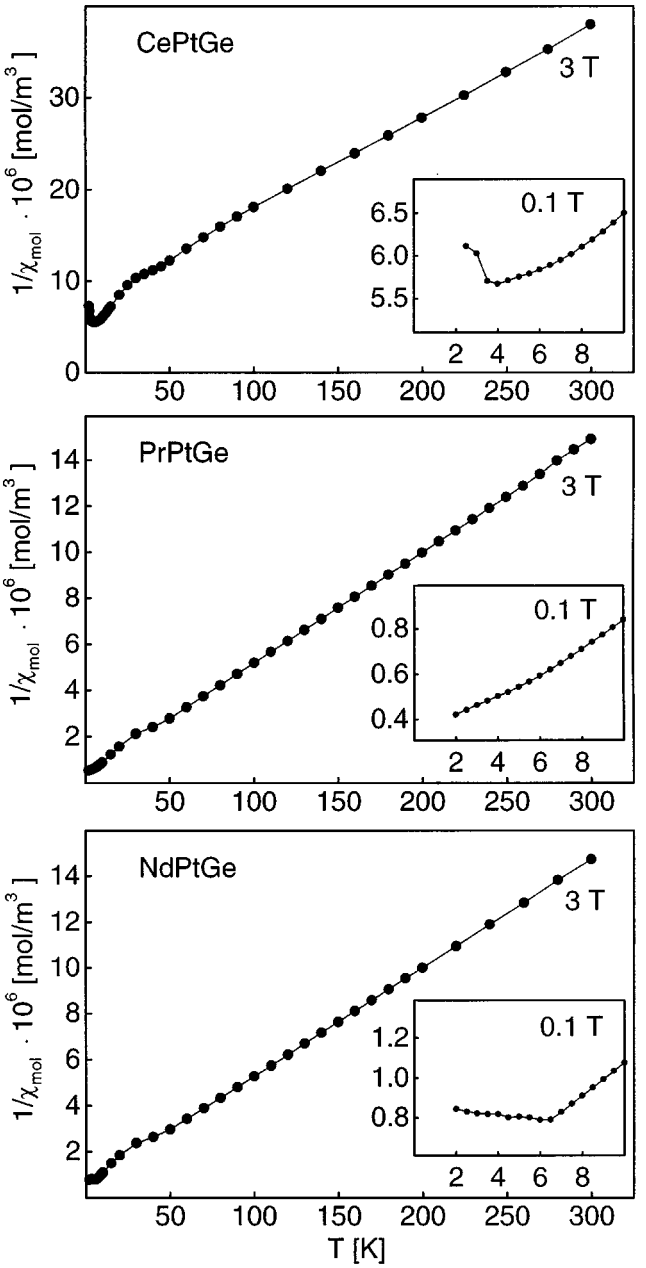

FIG. 1. Temperature dependence of the reciprocal susceptibilities of CePtGe, PrPtGe, and NdPtGe measured with a magnetic flux density of 3 T. The insets show the low temperature behavior recorded with a flux density of 0.1 T.

STRUCTURE REFINEMENTS

Irregularly shaped single crystals of CePtGe, PrPtGe, and α-SmPtGe were isolated from the annealed samples.

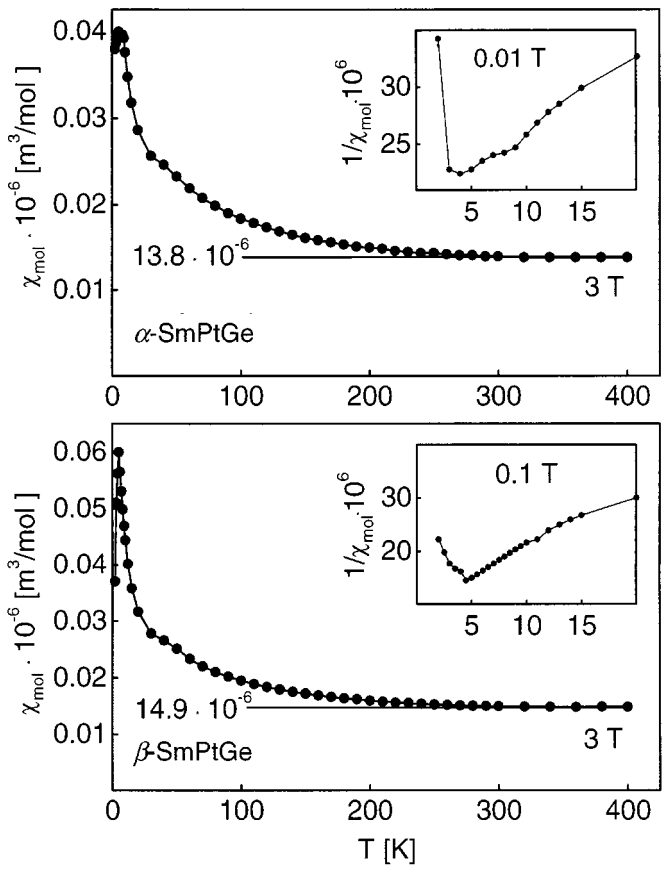

FIG. 2. Magnetic susceptibilities of the two modifications of SmPtGe determined with a magnetic flux density of 3 T. The insets show the reciprocal magnetic susceptibilities (m^3/mol) measured with lower magnetic flux densities.

The crystals of the high-temperature (β) modification of SmPtGe were obtained from a crushed arc-melted sample. They were investigated with Buerger precession and Weissenberg cameras. The crystals of CePtGe, PrPtGe, and α-SmPtGe showed primitive orthorhombic cells with a doubling of the *b* axes as compared to the KHg_2 type subcell, suggesting a YPdSi type structure (14). A cell corresponding to the body-centered cell of KHg_2 was also observed for the β-modification of SmPtGe. However, instead of the doubled *b* axis we found additional reflections violating the body-centering extinction condition of the KHg_2 type structure. This indicates a superstructure of the TiNiSi type, as has been observed earlier for this composition from powder data (1).

Single-crystal intensity data were collected at room temperature on a four-circle diffractometer (CAD4) with graphite-monochromatized Mo$K\alpha$ radiation and a scintillation counter with pulse-height discrimination. The scans were in the $\omega/2\theta$ mode, and background counts were recorded at both ends of each scan. Absorption corrections were applied on the basis of psi-scan data. Further details of the data collections are summarized in Table 3.

The atomic parameters of YPdSi (14) and TiNiSi (3), respectively, were used as starting parameters for the refinements of the structures. These full-matrix least-squares fits were carried out with the SHELXL-93 program system (23) using atomic scattering factors and anisotropic displacement parameters for all atoms. The weighting schemes and the corrections for isotropic secondary extinction were optimized by the program. The data of the α-SmPtGe crystal were strongly affected by absorption, as was indicated by the fact that all displacement parameters U_{11} were smaller than the corresponding parameters U_{22} and U_{33}. Some of the U_{11} parameters even tended to become negative. This was remedied by an additional absorption correction assuming spherical crystal shape.

As checks for the correct compositions and the correct atom assignments we refined the occupancy parameters of all atoms of the four structures together with the anisotropic displacement parameters, while the scale factors were fixed at the previously obtained values. These calculations were carried out with the least-squares program provided by the SDP system (24). The resulting occupancy values varied between 0.973(5) and 1.013(5) for the rare earth positions, between 0.989(2) and 1.014(2) for the platinum positions, and between 0.983(4) and 1.078(7) for the germanium positions. Thus, all occupancy parameters were close to the ideal values. Much larger deviations from the ideal occupancy values would be observed for substantial disorder. For instance, a mixed 50% Pt/50% Ge occupancy of a platinum or a germanium site should result in occupancy values of approximately 0.71 and 1.72, respectively, as calculated from the atomic numbers of these elements. Hence, in the final least-squares cycles—carried out again with the SHELXL-93 program system—the ideal occupancy values were resumed for all positions. Nevertheless, some evidence for disorder can be deduced from the refined occupancy values, as will be discussed below.

Although the structure refinements converged to low residuals for all reflections, we also calculated separate residuals for the superstructure reflections, since the overall residual is strongly affected by the strong subcell reflections. The low residuals for the superstructure reflections (Table 3) indicate that the models used for the refinement of the superstructures are correct. The final atomic parameters and interatomic distances are summarized in Tables 4 and 5. Listings of the anisotropic displacement parameters and the structure factor tables are available.[2]

[2]Details may be obtained from the Fachinformationszentrum Karlsruhe, D-76344 Eggenstein-Leopoldshafen (Germany), by quoting the Registry Numbers: CSD-410358 (CePtGe), CSD-410357 (PrPtGe), CSD-410350 (α-SmPtGe), and CSD-410349 (β-SmPtGe).

TABLE 3
Crystal Data for CePtGe, PrPtGe, and α- and β-SmPtGe

Empirical formula	CePtGe	PrPtGe	α-SmPtGe	β-SmPtGe
Structure type	YPdSi	YPdSi	YPdSi	TiNiSi
Molar mass	407.8	408.6	418.0	418.0
Space group	*Pmmn* (No. 59)	*Pmmn* (No. 59)	*Pmmn* (No. 59)	*Pnma* (No. 62)
Formula units per cell, Z	8	8	8	4
Lattice constants[a]				
a (pm)	444.9(1)	443.99(8)	439.49(5)	713.37(6)
b (pm)	1466.4(2)	1453.6(1)	1427.4(2)	438.57(7)
c (pm)	762.0(1)	761.4(1)	755.7(1)	759.5(1)
V (nm^3)	0.4971(1)	0.4914(1)	0.4741(1)	0.23762(5)
Calculated density (g/cm^3)	10.91	11.02	11.68	11.66
Crystal size (μm^3)	$10 \times 20 \times 40$	$10 \times 30 \times 40$	$10 \times 40 \times 60$	$20 \times 30 \times 60$
Transmission ratio (max/min)	1.61	3.77	2.62	3.21
2θ range up to	75°	66°	70°	65°
Range in *hkl*	$+7, \pm 25, -7 \leqslant l \leqslant 13$	$+6, -22 < k < 17, \pm 11$	$+7, \pm 23, \pm 12$	$\pm 10, -4 < k < 0, \pm 11$
Total no. of reflections	4824	3688	4470	1541
Independent reflections	1475	1026	1191	422
Internal residual on F^2 (R_i)	0.085	0.086	0.064	0.093
Reflections with $I > 2\sigma(I)$	710	579	742	352
No. of parameters	40	40	40	20
Overall residual $R(F)$	0.029	0.028	0.032	0.027
R (subcell reflections)[b]	0.023 (325)	0.022 (242)	0.025 (291)	0.025 (201)
R (superstructure reflections)[b]	0.045 (385)	0.039 (337)	0.043 (451)	0.031 (151)
Extreme residual peaks (e/nm^3)	−3802/5232	−4908/3833	−5792/7473	−3309/4268

[a] These lattice constants were obtained from the single-crystal diffractometer. The densities and interatomic distances have been calculated with the lattice constants determined from the Guinier powder data (Table 1).

[b] These residuals (on F) were calculated with the program RWERT (22) for the numbers of reflections indicated in parentheses.

DISCUSSION

The four compounds CePtGe, PrPtGe, NdPtGe, and α-SmPtGe have been reported earlier to crystallize with KHg_2 ($CeCu_2$) type structure, where the platinum and germanium atoms randomly occupy the mercury position of KHg_2 (1, 9–11). It is now clear that this structure represents only the subcell. In the YPdSi type superstructure (14), described here for these compounds, the platinum and germanium atoms are ordered, and as a result the *b* axis of the KHg_2 structure is doubled. The corresponding superstructure reflections were observed already in the quenched, arc-melted buttons of CePtGe, PrPtGe, and NdPtGe. In the case of the samarium compound the YPdSi type structure occurs for the low-temperature (α) form. Hence, annealing at 1070 K was necessary to obtain this modification. The quenched buttons of SmPtGe had the TiNiSi type structure, which also may be considered as a superstructure of the KHg_2 type (Fig. 3). In the case of the TiNiSi type structure (space group *Pnma*) the superstructure reflections are the reflections of the type $h + k + l = 2n + 1$, which violate the body-centered extinctions of the KHg_2 type structure (space group *Imma*).

Disorder is frequently reported for intermetallic compounds. In our opinion, at least short-range order can be expected in all such cases, except perhaps for samples, which have rapidly been quenched from high temperatures. In this context one should remember that evidence for long-range order in the form of superstructure reflections can be observed only if the ordered domains exceed 3000 to 5000 pm in diameter. This was studied in detail for the order–disorder transitions in Cu_3Au and CuZn a long time ago (25–28). And in these compounds the ordered arrangement occurs for elements with similar chemical potentials. Hence, it is not surprising that long-range order is observed for the greatly dissimilar platinum and germanium atoms of the equiatomic compounds LnPtGe already in the quenched arc-melted samples.

On the other hand, we have found some evidence for disorder in the YPdSi type germanides *Ln*PtGe during the least-squares refinements of the occupancy parameters. These occupancy parameters are listed in the second column of Table 4. It can be seen that, generally, most occupancy values correspond within three standard deviations to the ideal values. However, some larger deviations occur for the germanium positions in these compounds, e.g., the Ge1 position of CePtGe with 1.058(5), the Ge1 and Ge2 positions of PrPtGe with 1.078(7) and 1.038(6), and the Ge1 and Ge2 positions of α-SmPtGe with 1.063(8) and 1.046(8), respectively. The absolute values of the occupancy parameters cannot be determined, since they interrelate with the

TABLE 4
Atomic Parameters for CePtGe, PrPtGe, α-SmPtGe, and β-SmPtGe[a]

Atom	Occupancy	Site	x	y	z	U_{eq}
			CePtGe (space group *Pmmn*)			
Ce1	1.010(3)	4*e*	1/4	0.00274(6)	0.7910(2)	75(3)
Ce2	0.977(4)	2*b*	1/4	3/4	0.7093(3)	73(3)
Ce3	0.981(4)	2*a*	1/4	1/4	0.7040(3)	64(3)
Pt1	0.989(2)	4*e*	1/4	0.14122(4)	0.0801(2)	75(2)
Pt2	1.014(2)	4*e*	1/4	0.60011(4)	0.4173(2)	96(2)
Ge1	1.058(5)	4*e*	1/4	0.1006(1)	0.4119(4)	76(4)
Ge2	0.983(4)	4*e*	1/4	0.6558(1)	0.0880(4)	51(4)
			PrPtGe (space group *Pmmn*)			
Pr1	0.994(4)	4*e*	1/4	0.00259(6)	0.7928(2)	74(2)
Pr2	0.986(5)	2*b*	1/4	3/4	0.7094(2)	70(3)
Pr3	0.973(5)	2*a*	1/4	1/4	0.7047(2)	68(3)
Pt1	1.003(2)	4*e*	1/4	0.14150(3)	0.0812(1)	75(2)
Pt2	0.999(2)	4*e*	1/4	0.59889(4)	0.4175(2)	96(2)
Ge1	1.078(7)	4*e*	1/4	0.1004(1)	0.4122(4)	57(4)
Ge2	1.038(6)	4*e*	1/4	0.65556(9)	0.0882(3)	37(4)
			α-SmPtGe (space group *Pmmn*)			
Sm1	1.013(5)	4*e*	1/4	0.00209(6)	0.7919(1)	99(2)
Sm2	0.999(6)	2*b*	1/4	3/4	0.7089(2)	100(2)
Sm3	1.006(6)	2*a*	1/4	1/4	0.7053(2)	101(2)
Pt1	0.998(3)	4*e*	1/4	0.14188(4)	0.08109(9)	103(2)
Pt2	1.004(3)	4*e*	1/4	0.59866(4)	0.41759(9)	110(2)
Ge1	1.063(8)	4*e*	1/4	0.1009(1)	0.4119(2)	115(3)
Ge2	1.046(8)	4*e*	1/4	0.6549(1)	0.0894(2)	85(3)
			β-SmPtGe (space group *Pnma*)			
Sm	1.000(4)	4*c*	0.00347(8)	1/4	0.70416(8)	63(2)
Pt	1.004(3)	4*c*	0.29656(7)	1/4	0.41521(6)	68(2)
Ge	0.987(7)	4*c*	0.1888(2)	1/4	0.0870(2)	68(3)

[a] The equivalent isotropic displacement parameters U_{eq} (pm^2) are defined as one-third of the trace of the orthogonalized U_{ij} tensor. The occupancy parameters listed in the third column were obtained in separate refinement cycles. In the final least-squares cycles the ideal occupancy values were assumed.

overall scale factors. However, the relative values show a tendency that either there are some heavier atoms occupying the germanium sites or there are some lighter atoms at the platinum sites. The overall average occupancy parameters for these three compounds are 0.9932, 1.0012, and 1.0443 for the Ln, Pt, and Ge positions. Since the coordination polyhedra of the platinum and germanium atoms are similar, the most likely disorder is expected to occur for these atoms on their respective sites. The difference in the occupancy values of these two sites is 0.0431. This corresponds to an occupancy of the average germanium site by 3.0 at% Pt (the remainder being Ge). Alternatively, we can assume a different overall scale factor, e.g., we divide all average occupancy parameters by 1.0443. We then obtain the values 0.9511, 0.9587, and 1.000 for the occupancy parameters of the Ln, Pt, and Ge positions. A possible rationalization for these occupancy values would be the formation of vacancies on the lanthanoid sites and the occupancy of the platinum sites with germanium atoms. The occupancy value of 0.9587 would correspond to a Pt/Ge ratio of 92.7/7.3 at% for the average platinum site. A combination of these two different possibilities is also reasonable.

TABLE 5
Interatomic Distances in CePtGe, PrPtGe, and the Two Modifications of SmPtGe[a]

		CePtGe	PrPtGe	α-SmPtGe			CePtGe	PrPtGe	α-SmPtGe
Ln1:	1Pt1	299.4	298.7	296.2	Pt1:	2Ge2	257.6	257.6	255.7
	2Pt2	308.2	307.6	304.2		1Ge1	259.6	259.1	257.0
	2Ge1	310.4	310.1	306.2		1Ln1	299.4	298.7	296.2
	2Pt1	321.9	320.2	316.1		2Ln2	317.2	315.7	312.4
	1Pt2	322.1	321.8	317.6		1Pt1	318.7	316.1	308.8
	1Ge1	322.5	323.0	320.3		2Ln1	321.9	320.2	316.1
	1Ge2	324.3	322.0	317.7		1Ln3	327.8	327.5	323.6
	2Ge2	329.1	327.4	322.6	Pt2:	2Ge1	257.8	257.1	255.1
	1Ln3	368.2	366.6	360.0		1Ge2	263.8	264.1	261.0
	1Ln2	375.4	373.4	365.4		1Ge1	294.1	290.4	285.0
	2Ln1	388.6	386.0	384.2		2Ln1	308.2	307.6	304.2
	2Ln1	445.0	444.0	440.0		1Ln2	312.6	312.9	308.7
Ln2:	2Pt2	312.6	312.9	308.7		1Ln1	322.1	321.8	317.6
	4Pt1	317.2	315.7	312.2		2Ln3	326.0	326.2	322.1
	2Ge2	319.8	319.6	318.3	Ge1:	2Pt2	257.8	257.1	255.1
	4Ge1	325.4	324.6	319.5		1Pt1	259.6	259.1	257.0
	2Ln1	375.4	373.4	365.4		1Pt2	294.1	290.4	285.0
	2Ln3	385.5	385.7	382.9		2Ln1	310.4	310.1	306.3
	2Ln2	445.0	444.0	440.0		1Ln3	312.1	311.6	307.6
Ln3:	4Ge2	306.0	305.1	301.6		1Ln1	322.5	323.0	319.5
	2Ge1	312.1	311.6	307.6		2Ln2	325.4	324.6	320.3
	4Pt2	326.0	326.2	322.1	Ge2:	2Pt1	257.6	257.6	255.7
	2Pt1	327.8	327.5	323.6		1Pt2	263.8	264.1	261.0
	2Ln1	368.2	366.6	360.0		1Ge2	275.9	275.1	271.6
	2Ln2	385.5	385.7	382.9		2Ln3	306.0	305.1	301.6
	2Ln3	445.0	444.0	440.0		1Ln2	319.8	319.6	317.7
						1Ln1	324.3	322.0	318.3
						2Ln1	329.1	327.4	322.6

β-SmPtGe

Sm:	1Pt	303.3	Pt:	2Ge	255.6	Ge:	2Pt	255.6
	2Ge	303.6		1Ge	261.1		1Pt	261.1
	2Pt	307.0		1Ge	279.8		1Pt	279.8
	1Ge	315.3		1Sm	303.3		2Sm	303.6
	1Ge	319.7		2Sm	307.0		1Sm	315.3
	2Pt	319.7		2Sm	319.7		1Sm	319.7
	2Ge	322.9		1Sm	324.9		2Sm	322.9
	1Pt	324.9						
	2Sm	363.5						
	2Sm	380.2						
	2Sm	438.8						

[a] Standard deviations are all equal or less than 0.4 pm. All distances shorter than 480 pm (*Ln*–*Ln*), 400 pm (*Ln*–Pt, *Ln*–Ge), and 370 pm (Pt–Pt, Pt–Ge, Ge–Ge) are listed.

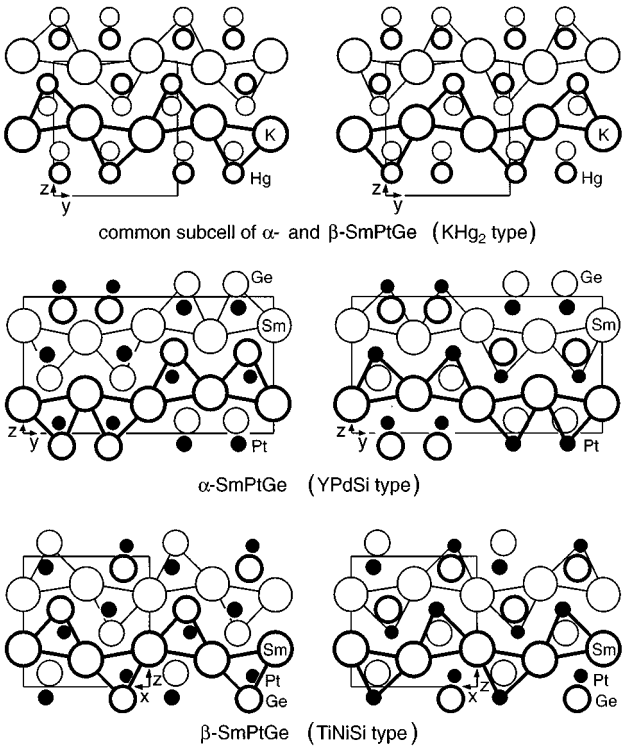

FIG. 3. The structures of the two modifications of SmPtGe as compared to their common subcell structure of KHg_2. Trigonal prisms around the germanium (right-hand side) and the transition metal atoms (left-hand side) are emphasized. These sites correspond to the (only one) mercury site of the body-centered KHg_2 ($CeCu_2$) type structure.

The cell volumes per formula unit V/Z of the presently reported germanides are plotted in Fig. 4 together with those of the other germanides *Ln*PtGe (1, 6, 7). For comparison we also show the values V/Z of the palladium silicides *Ln*PdSi, most of which we have investigated recently (14, 16, 17). These plots show the well-known lanthanoid contraction. The volumes of the europium compounds (6, 7, 29) are larger, indicating that the europium atoms are divalent. In general, the cell volumes per formula unit are not strongly dependent on the structure types. This is especially evident for the compounds with α-YbAuGe (CaCuGe), YPdSi, and TiNiSi type structure. These three structures are all superstructures with a KHg_2 type subcell (15, 16). A slight discrepancy occurs for the V/Z values of CePtGe and PrPtGe (YPdSi type) on the one hand and the corresponding silicides with PrPdSi type structure on the other hand. In this case the larger V/Z values of the silicides may be rationalized by the fact that the two structure types are quite different. Also, the V/Z values of the two lanthanum compounds differ slightly more than would be expected from the differences in the V/Z values of the compounds with the heavier lanthanoids. Such slight differences in the space filling of different structure types have already been noticed earlier for the two series *Ln*PtSi and *Ln*PtGe (1).

In Fig. 3 we compare the YPdSi and TiNiSi type structures occurring for the *Ln*PtGe compounds of the present communication. Both of these structure types are found for SmPtGe and both are superstructures of the KHg_2 type structure, which in turn may be considered as a superstructure of the well-known AlB_2 type structure. The group/subgroup relations of these structures have been presented in recent publications (14–16), together with those of various other related structures. The structures of silicides have frequently been classified by the way the trigonal prisms surrounding the small silicon atoms (augmented by three or four additional atoms outside the rectangular faces of the prisms) are linked to each other (e.g. 5, 30). In recent publications about similar structures of the compositions *LnTM* (T = transition metals, M = Si, Ge, Sn, In) we have emphasized the trigonal prisms containing the transition metal atoms (13–16, 31, 32). For the equiatomic compounds of the present publication these two points of view are completely equivalent, since both, the platinum and germanium atoms correspond to the mercury position of the KHg_2 type structure, as is demonstrated in Fig. 3.

The four structure types occurring for the whole series of rare earth platinum germanides *Ln*PtGe are projected in Fig. 5, emphasizing the polyanionic networks of the platinum and germanium atoms. One difference in these four structure types concerns the coordination numbers. As could be expected, the large lanthanum and europium atoms of LaPtGe and EuPtGe have higher coordination

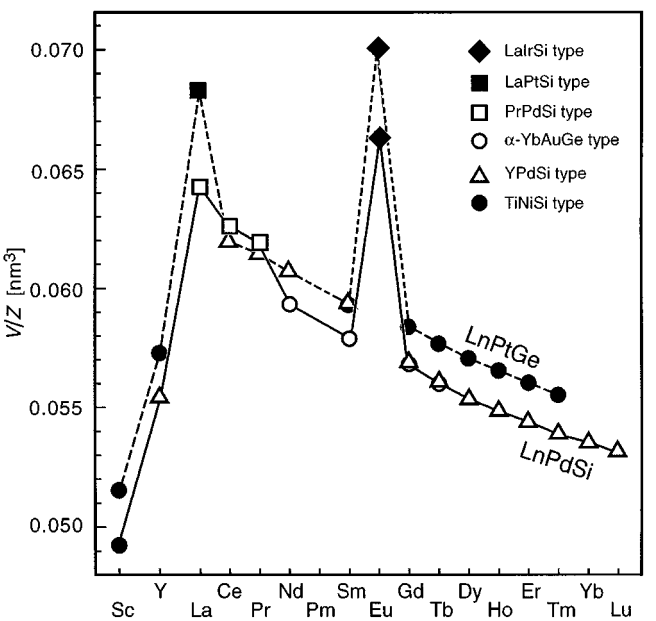

FIG. 4. Cell volumes per formula unit V/Z of ternary rare earth palladium silicides and platinum germanides *Ln*PdSi and *Ln*PtGe.

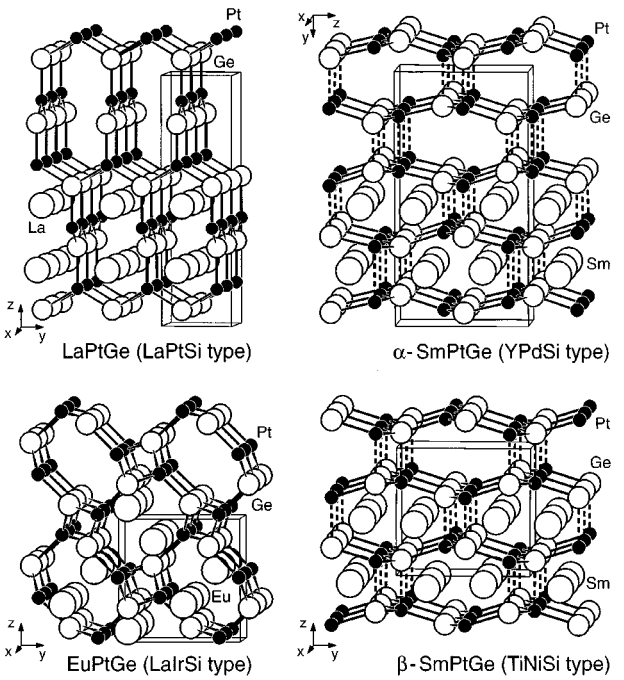

FIG. 5. Crystal structures of LaPtGe (tetragonal, LaPtSi type), EuPtGe (cubic, LaIrSi type), α-SmPtGe (orthorhombic, YPdSi type), and β-SmPtGe (orthorhombic, TiNiSi type). In the upper parts of each drawing the rare earth atoms are omitted for clarity. The platinum germanium polyanions are outlined. The weak interlayer interactions in α-SmPtGe and β-SmPtGe are drawn with dotted lines.

numbers (CN) than the samarium atoms in the two modifications of SmPtGe. In LaPtGe with LaPtSi type structure (2) the lanthanum atoms have CN 20 (6 Ge, 6 Pt, 8 La) and this is also the case for the europium atoms of EuPtGe with LaIrSi type structure (8), which have 7 Ge, 7 Pt, and 6 Eu neighbors. In contrast, the samarium atoms in both modifications of SmPtGe have CN 18 with 6 Ge, 6 Pt, and 6 Sm neighbors. It should be mentioned that some of the *Ln–Ln* distances are rather large. However, this is the case for all these structures. Another difference between the LaPtSi type structure of LaPtGe and the LaIrSi type structure of EuPtGe on one hand and the YPdSi and TiNiSi type structures of the other rare earth platinum germanides *Ln*PtGe on the other hand concerns the coordination numbers of the platinum and germanium atoms within the platinum germanium networks. In all of these four structure types the platinum and germanium atoms have three close neighbors of the other kind. However, while there are no further Pt–Ge interactions in the structures of LaPtGe and EuPtGe, additional weak interactions between these atoms occur in the structures of the other *Ln*PtGe compounds. For the latter we may take the structures of α- and β-SmPtGe as examples. In these, the three strong Pt–Ge interactions of each platinum and germanium atom (drawn with solid lines in Fig. 5) have bond lengths which vary between 255.1 and 261.1 pm. In addition, there are weak Pt–Pt (308.8 pm), Pt–Ge (285.0 pm), and Ge–Ge (271.6 pm) bonds in the structure of α-SmPtGe and weak Pt–Ge bonds (279.8 pm) in the structure of β-SmPtGe. These weak bonds are shown with dashed lines in Fig. 5. Without these weak bonds the platinum germanium networks in the YPdSi and TiNiSi type structures of α- and β-SmPtGe would consist of two-dimensionally infinite networks, while these networks are three-dimensionally infinite already without any additional Pt–Ge interactions in LaPtGe and EuPtGe. The bonding character of the weak Pt–Pt, Pt–Ge, and Ge–Ge interactions in α- and β-SmPtGe (dashed lines in Fig. 5) may be demonstrated indirectly by a comparison of the bond lengths of the strong Pt–Ge interactions of the four structure types. The structure of LaPtGe (1) has not been refined and therefore the precise Pt–Ge bond lengths are not known. However, the structure of EuPtGe has been refined recently (7). In this compound each platinum and each germanium atom has three neighbors of the other kind, all with the same Pt–Ge distance of 238.0(1) pm. This contrasts with the Pt–Ge distances of between 255.1 and 261.1 pm found in the present investigation for the three closest Pt–Ge interactions of the platinum and germanium atoms in α- and β-SmPtGe. Hence, the weak additional Pt–Pt, Pt–Ge, and Ge–Ge interactions in both modifications of SmPtGe considerably reduce the bond strengths of the strong Pt–Ge interactions.

Almost always the high-temperature modification of a solid state compound has higher symmetry than the low-temperature modification, regardless whether the phase transition is of a displacive or a diffusion-controlled type. This has recently been pointed out for the two modifications of GdPdSi and TbPdSi (16) and is also the case for α- and β-SmPtGe. Both modifications of SmPtGe crystallize with a primitive lattice with the Laue symmetry *mmm*. The general positions of the space groups (*Pmmn* and *Pnma*) are eightfold in both cases. However, the unit cell of the low-temperature modification contains a larger number of atomic positions ($Z = 8$) than that of the high-temperature form ($Z = 4$). Hence, a larger number of positional parameters need to be determined for α-SmPtGe than for β-SmPtGe (Table 4).

ACKNOWLEDGMENTS

We thank Dipl.-Ing. Ute Ch. Rodewald for the data collections on the four-circle diffractometer and Klaus Wagner for the EDX analyses. Special thanks go to Dr. Wolfgang Gerhartz (Degussa AG) and Dr. G. Höfer (Heraeus Quarzschmelze) for generous gifts of platinum powder and silica tubes. This work was financially supported by the Benningsen-Foerder-Programm of the Ministerium für Wissenschaft und Forschung des Landes Nordrhein–Westfalen, the Fonds der Chemischen Industrie, and the Deutsche Forschungsgemeinschaft. Yu.M.P. is indebted to the DAAD and the Heinrich-Hertz-Stiftung for research stipends.

REFERENCES

1. E. Hovestreydt, N. Engel, K. Klepp, B. Chabot, and E. Parthé, *J. Less-Common Met*. **85,** 247 (1982).
2. K. Klepp and E. Parthé, *Acta Crystallogr. Sect. B* **38,** 1105 (1982).
3. C. B. Shoemaker and D. P. Shoemaker, *Acta Crystallogr.* **18,** 900 (1965).
4. V. Johnson and W. Jeitschko, *J. Solid State Chem.* **4,** 123 (1972).
5. E. Parthé and B. Chabot, *in* "Handbook on the Physics and Chemistry of Rare Earths" (K. A. Gschneidner, Jr. and L. Eyring, Eds.), Vol. 6, pp. 113–334. North-Holland, Amsterdam, 1984.
6. J. Evers, G. Oehlinger, K. Polborn, and B. Sendlinger, *J. Less-Common Met*. **182,** L23 (1992).
7. R. Pöttgen, R. K. Kremer, W. Schnelle, R. Müllmann, and B. D. Mosel, *J. Mater. Chem.* **6,** 635 (1996).
8. K. Klepp and E. Parthé, *Acta Crystallogr. Sect. B* **38,** 1541 (1982).
9. Yu. M. Prots', V. V. Pavlyuk, G. M. Barakatova, O. I. Bodak, and J. Stępień-Damm, *Z. Kristallogr.* **210,** 902 (1995).
10. P. Rogl, B. Chevalier, M. J. Besnus, and J. Etourneau, *J. Magn. Magn. Mater*. **80,** 305 (1989).
11. A. V. Gribanov, Y. D. Seropegin, O. I. Bodak, V. N. Nikiforov, A. A. Velikhovskii, and J. Mirkovic, *J. Phase Equilibria* **17,** 196 (1996).
12. R. Pöttgen, *J. Mater. Chem.* **5,** 505 (1995).
13. R. Pöttgen, R.-D. Hoffmann, R. Müllmann, B. D. Mosel, and G. Kotzyba, *Chem. Eur. J*. **3,** 1852 (1997).
14. Yu. M. Prots', R. Pöttgen, and W. Jeitschko, *Z. Anorg. Allg. Chem.* **624,** 425 (1998).
15. D. Kußmann, R.-D. Hoffmann, and R. Pöttgen, *Z. Ànorg. Allg. Chem.* **624,** 1727 (1998).
16. Yu. M. Prots' and W. Jeitschko, *J. Solid State Chem.* **142,** 130 (1999).
17. Yu. M. Prots', W. Jeitschko, M. Gerdes, and B. Künnen, *Z. Anorg. Allg. Chem.* **624,** 1855 (1998).
18. D. Niepmann, R. Pöttgen, Yu. M. Prots', and W. Jeitschko, *Z. Kristallogr. Suppl.* **15,** 49 (1998).
19. K. Yvon, W. Jeitschko, and E. Parthé, *J. Appl. Crystallogr.* **10,** 73 (1977).
20. J. H. Van Vleck, "The Theory of Electric and Magnetic Susceptibilities." Oxford Univ. Press, Oxford, 1932.
21. A. S. Borovik-Romanov and N. M. Kreines, *Sov. Phys. JETP* **2,** 657 (1956).
22. R.-D. Hoffmann, RWERT, Program for the Calculation of Residual Values for Specific Classes of Reflections. University of Münster, Germany, 1996.
23. G. M. Sheldrick, SHELXL-93, Program for Crystal Structure Refinement. University of Göttingen, Germany, 1993.
24. B. A. Frenz and Associates Inc. and Enraf-Nonius, SDP (Structure Determination Package). Version 3. College Station, TX/Delft, 1985.
25. F. C. Nix and W. Shockley, *Rev. Mod. Phys.* **10,** 1–71 (1938).
26. B. E. Warren, "X-Ray Diffraction." Addison–Wesley, Reading, MA, 1969.
27. B. D. Cullity, "Elements of X-Ray Diffraction," 2nd ed. Addison–Wesley, Reading, MA, 1959.
28. C. S. Barrett and T. B. Massalski, "Structure of Metals," 3rd rev. ed. Pergamon, Oxford, 1980.
29. J. Evers, G. Oehlinger, K. Polborn, and B. Sendlinger, *J. Solid State Chem.* **91,** 250 (1991).
30. E. I. Gladyshevskii and Yu. N. Grin', *Sov. Phys. Crystallogr.* **26,** 683 (1981).
31. R. Pöttgen, *Z. Naturforsch. B* **51,** 806 (1996).
32. R. Pöttgen, *Z. Kristallogr.* **211,** 884 (1996).